Published in final edited form as:
Clin Pharmacol Ther. 2010 May ; 87(5): 579–585. doi:10.1038/clpt.2010.11.

Regional P-glycoprotein Activity and Inhibition at the Human Blood-Brain Barrier as Imaged by Positron Emission Tomography

Sara Eyal[1], **Ban Ke**[1], **Mark Muzi**[2], **Jeanne M. Link**[2], **David A. Mankoff**[2], **Ann C. Collier**[3], and **Jashvant D. Unadkat**[1]

[1]Department of Pharmaceutics, University of Washington, Seattle, Washington

[2]Division of Nuclear Medicine, University of Washington, Seattle, Washington

[3]Department of Medicine, University of Washington and Seattle Cancer Care Alliance, Seattle, Washington

Abstract

We evaluated the contribution of P-glycoprotein (P-gp) at the human blood-brain barrier (BBB) to regional brain drug distribution using positron emission tomography (PET). Eleven healthy volunteers underwent PET imaging with [^{11}C]-verapamil before and during cyclosporine A infusion. Regional P-gp inhibition was expressed as cyclosporine A-induced percent change in the brain distributional clearance of verapamil (K_1) normalized to the regional blood flow (rCBF). K_1 estimates were similar across grey matter regions, lower in the white matter, but all were considerably lower than rCBF. Normalization of K_1 by rCBF diminished the grey-to white matter differences. In contrast, the K_1 for the pituitary, which resides outside the BBB, approximated rCBF. The magnitude of P-gp inhibition was comparable across BBB-protected brain structures. Our results indicate that P-gp and its inhibition will equally affect the distribution of drugs (and therefore their neuroefficacy and toxicity) in the different brain regions protected by the BBB.

Keywords

P-glycoprotein; blood-brain barrier; verapamil; cyclosporine; cerebral blood flow; PET imaging

Introduction

The multidrug resistance protein, P-glycoprotein (P-gp; encoded by *ABCB1*) is highly expressed at the apical membrane in brain capillary endothelial cells that form the blood-brain barrier (BBB). P-gp is considered to be the most important efflux transporter at the BBB, because its high expression there and its ability to exclude a wide variety of drugs from the CNS, including antiretroviral drugs, cancer chemotherapeutic agents and antibiotics [1,2]. Drug removal protects the CNS from potential neurotoxic effects, but also prevents effective pharmacotherapy of neurological diseases [1]. More recently, it has been suggested that P-gp plays a role in regulating CNS levels of toxins associated with Parkinson's disease and of amyloid-β, a causative factor in the development of Alzheimer's disease [3,4].

Address correspondence to: Dr. Jashvant D. Unadkat, Department of Pharmaceutics, University of Washington, Box 357610, Seattle, WA 98195, Telephone: 206-543-9434, Fax: 206-543-3204, jash@u.washington.edu.

The authors declare no conflict of interest.

By contributing to the protective function of the BBB, P-gp helps maintain an optimal extracellular environment for neuronal activity. It is therefore not surprising that local abnormalities of P-gp expression and/or function have been increasingly associated with neurological disorders [5]. P-gp has been reported to be overexpressed in capillary endothelial cells of epileptogenic brain tissue in the neocortex and the hippocampus of patients with medically refractory epilepsy [6–8]. Recently, results from a positron emission tomography (PET) study in patients with major depression suggested enhanced BBB P-gp activity throughout the brain, and in particular in the frontal and temporal regions [9]. Using the same imaging technique, Parkinson's disease has been associated with impaired BBB P-gp function in the midbrain and frontal white matter [3,10]. In brains obtained postmortem from elderly humans, P-gp expression in medial temporal lobe vessels correlated inversely to deposition of amyloid-β [11]. In addition, BBB P-gp activity appears to decrease regionally during aging [12–14].

Whether P-gp activity is uniform throughout the human BBB is currently unknown. This question is clinically relevant, because some P-gp substrates have non-uniform CNS distribution or produce effects that may not be explained by regional-selective receptor binding. For example, substrates such as colchicine [15] and digoxin [16] are neurotoxic in some brain regions, but not in others [17,18]. Furthermore, it is important to understand whether inhibition of P-gp at the BBB, whether intended or not, will results in comparable magnitude of increases in drug concentrations in all regions of the brain.

We have previously assessed in healthy volunteers the effect of P-gp inhibition by cyclosporine on whole brain distribution of [^{11}C]-verapamil, an established P-gp substrate. Over 20 min, cyclosporine increased the whole brain-to-plasma ratio of the area under the concentration-time curve (AUCR) of [^{11}C]-verapamil radioactivity by 88% [19]. Compartmental analysis indicated that inhibition of P-gp at the BBB by cyclosporine manifests as an increase in distributional clearance (K_1) of [^{11}C]-radioactivity into the brain [20]. Furthermore, transport estimates from a 1-tissue compartment model using the first 10 minutes of data correlated to those from a 2-tissue compartment model, indicating that a short study could effectively estimate K_1 [20].

Here, we report for the first time a PET imaging study where we have measured regional P-gp activity at the human BBB and the impact of its inhibition. To account for regional differences in cerebral blood flow, regional P-gp activity was expressed as the distributional clearance, K_1, normalized to the regional blood flow (rCBF) (often referred to as extraction ratio, ER, [21] or extraction fraction [22]). Brain tissue exposure to the tracer (AUCR) further served as a reciprocal estimate of BBB P-gp activity. The impact of P-gp inhibition by cyclosporine was described as percent change in these parameters.

Results

Of the 12 subjects enrolled in the studies, regional BBB P-gp activity was evaluated in eleven for whom MR images for this analysis were available. Nine subjects provided DNA samples and were genotyped for *ABCB1*. The clinical outcomes of the study, as well as the lack of effect of cyclosporine on plasma [^{11}C]-radioactivity, [^{11}C]-verapamil metabolism and plasma protein binding have been previously reported [19].

The brain distribution of [^{11}C]-radioactivity before and during cyclosporine administration in a representative subject are shown in Fig. 1. Clearly, irrespective of the presence of cyclosporine, there was greater distribution of [^{11}C]-radioactivity into the pituitary and the choroid plexus (red regions) than into BBB-protected regions, and greater distribution of radioactivity into the grey matter (green-to-yellow regions) than into the white matter (dark

blue regions). Correspondingly, the mean baseline (before cyclosporine) distributional clearance of radioactivity (K_1) was greater into the grey matter than into the white matter (0.066 ± 0.011 mL/min/g and 0.029 ± 0.006 mL/min/g, respectively, $P < .05$; Fig. 2A).

The mean baseline K_1 values of grey matter regions did not significantly differ from each other and ranged from 0.057 ± 0.010 mL/min/g in the thalamus to 0.074 ± 0.008 mL/min/g in the occipital cortex (Fig. 2A). In contrast, the baseline K_1 estimates for the pituitary (0.282 ± 0.058 mL/min/g) and the choroid plexus (0.132 ± 0.032 mL/min/g) were significantly greater ($P < .01$) than those of the lateral temporal cortex (0.059 ± 0.010 mL/min/g) or the thalamus.

Infusion of cyclosporine (at average pseudo-steady state blood concentrations 2.8 ± 0.4 μmol/L) significantly increased ($P < .01$) the K_1 value of each brain region studied (Fig. 2A). The magnitude of increase in grey matter structures ranged from 63 ± 29% in the caudate nucleus to 97 ± 49% in the thalamus, and, except for caudate nucleus vs. the thalamus ($P < .05$), did not significantly differ between grey and white matter or across BBB-protected structures (Fig. 2D). In addition, the magnitude of change in the pituitary (28 ± 14%) or the choroid plexus (50 ± 21%) was significantly smaller than in the thalamus or the lateral temporal cortex (86 ± 3%).

The rank order of the [^{11}C]-radioactivity AUCR values for the various regions of the brain was similar to that of K_1, regardless of cyclosporine administration (Fig. 2B). With the administration of cyclosporine, the magnitudes of change in the AUCR were similar to those of K_1 (Fig. 2D). Moreover, with the exception of the pituitary, individual AUCRs before and during cyclosporine administration correlated well with the corresponding K_1 estimates for each brain region ($r > 0.85$, $P < 0.001$, data not shown).

In each of the BBB-protected brain regions, the distributional clearance of [^{11}C]-radioactivity remained well below rCBF in both the absence and the presence of cyclosporine. Accordingly, the tracer ER (K_1/rCBF) ranged from 0.14 ± 0.05 to 0.20 ± 0.07 and 0.21 ± 0.04 to 0.30 ± 0.07 before and during cyclosporine administration, respectively, representing poor permeability of [^{11}C]-radioactivity across the BBB (due to P-gp activity) (Fig 2C). In contrast, the pituitary ERs in both the absence and the presence of cyclosporine were 1.12 ± 0.66 and 1.12 ± 0.44, respectively. The grey and white matter ER estimates did not appear to be associated with any of the studied *ABCB1* SNPs (Table 1). With the administration of cyclosporine, the ER significantly increased in all the BBB-protected brain structures, but not in the choroid plexus and the pituitary. The mean ER (Fig. 2C) as well as the magnitude of cyclosporine-induced change in this parameter (Fig. 2D) did not significantly differ across BBB-protected brain structures. In addition, the change in ER in the white and grey matter was not significantly different. Furthermore, the change in ER across the studied grey matter brain structures (with the exception of the pituitary) correlated modestly-to-well with each other, indicating proportional cyclosporine-induced increases in the ER across brain regions of the same individual (data not shown). None of the estimated parameters correlated with the age of the subject, which ranged from 20 to 50 years (data not shown).

Discussion

The goal of this study was to determine if P-gp activity at the human BBB differs between distinct brain regions. In this report we demonstrate for the first time that P-gp activity is fairly uniform in all brain regions protected by the BBB while it is negligible or not present in the pituitary which resides outside the BBB. In addition, the ability of cyclosporine to inhibit P-gp is uniform within the regions protected by the BBB.

We have previously shown, using [^{11}C]-verapamil as the P-gp substrate and cyclosporine as the P-gp inhibitor, that P-gp inhibition primarily increases the influx of [^{11}C] radioactivity into

the brain (K_1) rather than decreases its efflux from the CNS (k_2) [20]. Those findings are consistent with the "vacuum cleaner" hypothesis for the mechanism of action of P-gp where P-gp effluxes drug directly from the lipid bilayer before it enters the cytoplasmic compartment of a cell [5]. This hypothesis is supported by biochemical data [23–26] as well as the recent three dimensional crystal structure of P-gp [27]. The impact of P-gp inhibition was described as percent change in K_1 or AUCR, which increases with the magnitude of P-gp contribution to tracer distribution into the tissue [5]. Furthermore, the excellent correlation between K_1 and AUCR indicates that they can both be used when P-gp activity in BBB-protected regions is estimated by [^{11}C]-verapamil. Since we also measured rCBF, K_1 can be corrected for differences in rCBF to provide an estimate of P-gp activity uninfluenced by variation in delivery due to differences in rCBF. The ratio K_1/rCBF provides a measure of the ability of each region to extract the tracer (i.e. extraction ratio or extraction fraction) and serves as an overall measure of the permeability of the BBB in various regions of the brain. Since P-gp transport affects the distributional clearance of verapamil into the brain, i.e, the apparent permeability, this ratio serves as a useful index of P-gp function. Under restrictive clearance conditions, this ratio remains dependent on plasma protein binding of verapamil and rCBF, but under non-restrictive clearance, this ratio is independent of these factors and approaches the value of unity [21].

In the absence of P-gp inhibition, the uptake of [^{11}C]-radioactivity into grey and white matter was low (AUCR < 0.5), consistent with P-gp activity at the BBB preventing entry of verapamil radioactivity into the brain. The K_1 and AUCR of [^{11}C]-radioactivity were comparable across the analyzed grey matter structures, suggesting similar rate and extent of drug transfer and/or, binding (specific and non-specific) in those tissues. These parameters (K_1 and AUCR) were higher for the grey matter regions than the white matter; however, as expected [28,29], the rCBF for the grey matter regions was also higher than for the white matter. When verapmil K_1 is adjusted for blood flow to compute the regional ER, the difference between grey and white matter becomes minimal, and reflects low transport of verapamil to areas well-protected by the BBB, where P-gp is active. However, the ER for the choroid plexus and pituitary is much higher. This is not surprising as the blood-choroid plexus and the blood-neurohypophysis boundary is leakier (assuming that the observed tracer kinetics represent the posterior pituitary that resides outside the BBB). This permeability difference between the pituitary/choroid plexus and brain tissue has also been demonstrated for another P-gp substrate, [^{11}C]-N-desmethyl-loperamide [30].

In the choroid plexus, P-gp is thought to be located on the apical (i.e. CSF side) membrane of the choroid plexus epithelial cells [31,32]. Therefore, inhibition of choroid plexus P-gp by cyclosporine should either increase or not change the [^{11}C]-radioactivity content of the tissue. This is exactly what was observed. Similarly, cyclosporine did not change the ER of verapamil by the pituitary, a structure outside of the BBB. On the contrary, in the presence of cyclosporine, the ER for all BBB-protected brain structures increased due to inhibition of P-gp.

In the presence of cyclosporine, the percent change in ER of [^{11}C]-radioactivity for all brain regions protected by the BBB ranged from 51% to 84% (caudate nucleus to thalamus). Clearly, this is a modest change when compared with rodents where P-gp has been genetically or chemically disabled (~1000% increase; [33,34]). Due to concerns of toxicity, higher dose of cyclosporine cannot be administered to humans to chemically ablate P-gp. Therefore, it is not clear what the maximum percent increase in the brain distribution of [^{11}C]-radioactivity would be if P-gp were to be chemically disabled at the human BBB. This key question needs to be addressed before strategies to deliberately inhibit P-gp at the human BBB are pursued. Based on our data, we speculate that the distribution of [^{11}C]-radioactivity after administration of verapamil (or any other lipophilic) drug will be limited by rCBF in that region. Thus we expect that, on maximum inhibition of P-gp, the ER of [^{11}C]-verapamil by the BBB-protected regions

will increase by ~5-fold. This speculation is supported by our observation that distribution clearance of [^{11}C]-radioactivity into the pituitary (K_1) approaches the rate of blood flow to this brain region. In addition, the change in K_1 during cyclosporine administration appears to correspond with the cyclosporine-induced change in rate of blood flow to this region (28% vs. 29%, respectively). Data in the literature support this assertion. In non-human primates, complete P-gp inhibition increased the distributional clearance (K_1) of [^{11}C]-N-desmethyl-loperamide-radioactivity into the brain by 5-fold, and K_1 approached rCBF. In addition, when corrected for blood flow, the distribution of [^{11}C]-N-desmethyl-loperamide-radioactivity across various brain structures was uniform [22]. Likewise, complete inhibition of P-gp in the non-human primates increased the brain distribution of [^{11}C]-verapamil by up to 5-fold [35–37].

Although in the current study we used racemic verapamil, that undergoes stereoselective metabolism [5,38,39], verapamil R and S enantiomers have approximately equal affinity for P-gp [40]. Therefore, as discussed in previous publications [36,41], the only contributors to the regional distribution of [^{11}C]-verapamil-radioactivity into the brain are the total [^{11}C]-verapamil blood concentration and the regional BBB P-gp activity.

Nine of the subjects that took part in this study were genotyped for *ABCB1* single nucleotide polymorphisms (Table 1). The synonymus C3435CT and C1236T polymorphisms, together with the missense G2677T/A mutation, encode a haplotype protein with altered structure that is less responsive to some P-gp modulators, including cyclosporine [42], whereas the missense mutation G1199A alters P-gp's transport activity [43,44]. Due to the small sample size we could not conduct any statistical analysis to determine the influence of these polymorphisms on regional P-gp activity. However, previous imaging studies in healthy volunteers with [^{11}C]-verapamil have found no effect of polymorphisms in the MDR gene on the brain uptake of [^{11}C]-radioactivity [14,45]. As previously discussed [19], the inter-individual variability in baseline AUCR or ER (Fig. 2) suggests that P-gp activity at the human BBB is tightly regulated.

In conclusion, P-gp plays an important role in limiting substrate delivery into BBB-protected brain regions. Our data suggest that in the absence of functional P-gp, the rate of substrate uptake into the brain may be limited by delivery, i.e., rCBF. P-gp inhibition occurs throughout the human brain. The magnitude of inhibition is comparable across BBB-protected structures and P-gp inhibition results in comparable substrate accumulation in those brain regions of a given healthy individual. For example, P-gp inhibition in patients with pharmacoresistant epilepsy, aimed to increase the concentrations of anticonvulsants such as phenytoin, carbamazepine and lamotrigine in seizure foci in lateral temporal lobe, might result in equally greater drug concentrations in the cerebellum and subsequent cerebellar toxicity (e.g., ataxia and nystagmus) [46] . In this study, cyclosporine inhibited P-gp to modestly increase the brain distribution of [^{11}C]-verapamil. However, even this modest inhibition of P-gp could result in neurotoxicity if the drug has a narrow therapeutic window. In addition, such inhibition could result in much greater increase in the brain distribution of other P-gp substrates, particularly those with higher P-gp affinity (e.g. nelfinavir) [6–8]. Therefore, additional PET studies in humans with such substrates and with other more potent P-gp inhibitors are warranted.

Methods

Subjects

Subject characteristics have been previously described by Sasongko et al [19]. Briefly, six male and six female healthy volunteers (20–50 years old) were enrolled in the studies. The protocols were approved by the University of Washington Human Subjects, Radiation Safety and the Radioactive Drug Research Committees. All subjects provided signed informed consent.

PET Imaging

Radiosynthesis methods and study design have been previously published [19] and therefore are described here briefly. Venous lines were placed for [^{11}C]-verapamil and cyclosporine administration and arterial catheters were inserted for blood sampling. Images were acquired as 3D dynamic emission scans on an Advance Tomograph (GE Healthcare, Waukesha, WI). A 20 min transmission scan by use of a rotating germanium-68 source was followed by a sequence of 5 substudies, as described below.

[^{15}O]-water (<0.54 mCi/kg or up to 40 mCi) was administered as an intravenous bolus to measure regional blood flow. Images were acquired and arterial blood samples (1 mL) were obtained as described in Fig. 3. Blood and plasma radioactivity was measured by a gamma counter (Cobra Counter; Packard Corporation, Meriden, Conn).

Approximately 15 min after the [^{15}O]-water administration, [^{11}C]-verapamil (~0.2 mCi/kg or up to 0.12 μg/kg) was administered intravenously over 1 min. Image acquisition was conducted for up to 45 min after injection and blood samples (1 mL) were taken to match the imaging sequence (Fig. 3). Aliquots of 100 μl of blood and 100 μl of plasma were counted. A larger volume of blood (3–5 mL) was collected at 0, 1, 5, 10, 15, 20 and 45 min to determine plasma [^{11}C]-verapamil and metabolite concentrations as previously described [47].

Cyclosporine infusion (2.5 mg/kg/h, UWMC Drug Services) was initiated after completion of the first [^{11}C]-verapamil study and continued during the second [^{11}C]-verapamil and [^{15}O]-water study. The [^{15}O]-water and [^{11}C]-verapamil imaging sub-studies were repeated at ~45 and ~1 h, respectively, after beginning the cyclosporine infusion. Blood samples were taken at 15, 30, 45, 60, 90 and 120 min following the start of cyclosporine infusion to measure cyclosporine concentrations by HPLC//UV absorbance detection [19].

At the end of the second [^{11}C]-verapamil study, [^{11}C]-CO (~0.2 mCi/kg) was administered by inhalation to determine cerebral blood volume. Images were acquired for 16 min after inhalation, and radioactivity was measured in blood samples (1 mL) taken every 4 min (Fig. 3). The subject had a MRI scan within 2 weeks of the PET study to provide anatomical information for constructing regions-of-interest (ROI).

Image reconstruction and analysis

PET images were reconstructed using a 3D reconstruction algorithm with correction for scattered and random coincidences. The tomograph, dose calibrator, and gamma counter were cross-calibrated to express all measurements in common units of radioactivity (Bq/cc). MRI images (T1) were co-registered to the PET images by use of PMOD Version 2.9 (PMOD Technologies, Zurich, Switzerland). Regions of interest (ROIs) for grey matter, white matter, frontal cortex, lateral temporal cortex, parietal cortex, occipital cortex, caudate nucleus, putamen, thalamus, cerebellar cortex, pituitary and choroid plexus were identified on the co-registered MR images. These larger brain regions were chosen based on their importance in the efficacy and neurotoxicity of therapeutic compounds, as well as our ability to model the data obtained with confidence while avoiding partial volume effects (except for the pituitary). Thus, structures such as the hippocampus and the ventricles were excluded from our analysis due to spill-in from the choroid plexus. The ROIs from contiguous slices were combined to create volumes of interest (VOI) for each tissue type. VOIs were applied to both the dynamic image sets and the static summed SUV images (5–25 min for [^{11}C]-verapamil, 20–80 sec for [^{15}O]-water, and 4–16 min for [^{11}C]-CO) for data extraction. The pituitary VOI was created around the apparent center of the gland and consisted of 4-pixel (~12 × 12 mm) ROIs on 2 sequential slices. Partial volume correction was not applied to avoid overestimation of radioactivity due to the proximity of the portal blood system. However, the percent change in

the estimated parameters with cyclosporine administration vs. baseline as well as the ER are not affected by a partial volume effect, because this was a within-subject comparison. All the other brain regions were larger than three times the effective size-resolution of the reconstructed image (> 3 × 0.6 cm), and did not require partial volume correction.

Image and blood data were decay-corrected to the injection time. A 1-compartment model was implemented on a subset of the data (0–10 min) for estimation of the plasma-to-brain distributional clearance of total [^{11}C]-radioactivity (K_1), applying the regional blood volume obtained from the [^{11}C]-CO study as a fixed parameter in the model (PMOD) [20]. As before [20], in fitting the 1-compartment model to the data, we assumed that verapamil and its lipophilic radiolabeled metabolites (D617/717 that are P-gp substrates) behave similarly. Furthermore, at 10 min the overall contribution of radiolabeled metabolites to total plasma radioactivity is < 20% [47]. Vascular volume-corrected tissue and blood area under the concentration-time curves (AUC) were calculated by use of the trapezoidal rule. Then the ratio between the vascular volume-corrected tissue AUC and blood AUC over the first 10 min of scan, designated as AUCR, was calculated and used as an additional index of P-gp activity. Cerebral blood flow was estimated using a 1-compartment model as previously described [20].

Genotyping methods

Bucal cell isolation and genotyping method were described by Hebert et al [48]. *ABCB1* G1199A, C1236T, and C3435T single-nucleotide polymorphisms were determined using validated TaqMan assays from Applied Biosystems (Foster City, CA). G2677T/A single-nucleotide polymorphisms were determined as described previously [49].

Statistical analysis

Data are expressed as mean ± SD. Statistical analysis was performed using InStat 3 (GraphPad Software, La Jolla, CA, USA). Repeated measures ANOVA, followed by Bonferroni's test for multiple comparisons, was used for statistical comparisons across brain regions. Grey matter was compared to white matter using a paired t-test. The significance level was set at $P < .05$

Acknowledgments

We thank Jeff Stevenson from UW Department of Radiology and Tot Bui Nguyen and Dr. Edward Kelly from the UW Department of Pharmaceutics for their expert technical assistance and the DNA Sequencing and Gene Analysis Center at UW School of Pharmacy.

This study has been supported by NIA Grant R33 AG031485.

References

1. Eyal S, Hsiao P, Unadkat JD. Drug interactions at the blood-brain barrier: fact or fantasy? Pharmacol Ther 2009;123:80–104. [PubMed: 19393264]
2. Schinkel AH. P-Glycoprotein, a gatekeeper in the blood-brain barrier. Adv Drug Deliv Rev 1999;36:179–194. [PubMed: 10837715]
3. Bartels AL, Willemsen AT, Kortekaas R, de Jong BM, de Vries R, de Klerk O, et al. Decreased blood-brain barrier P-glycoprotein function in the progression of Parkinson's disease, PSP and MSA. J Neural Transm 2008;115:1001–1009. [PubMed: 18265929]
4. Cirrito JR, Deane R, Fagan AM, Spinner ML, Parsadanian M, Finn MB, et al. P-glycoprotein deficiency at the blood-brain barrier increases amyloid-beta deposition in an Alzheimer disease mouse model. J Clin Invest 2005;115:3285–3290. [PubMed: 16239972]
5. Kannan P, John C, Zoghbi SS, Halldin C, Gottesman MM, Innis RB, et al. Imaging the function of P-glycoprotein with radiotracers: pharmacokinetics and in vivo applications. Clin Pharmacol Ther 2009;86:368–377. [PubMed: 19625998]

6. Aronica E, Gorter JA, Ramkema M, Redeker S, Ozbas-Gerceker F, van Vliet EA, et al. Expression and cellular distribution of multidrug resistance-related proteins in the hippocampus of patients with mesial temporal lobe epilepsy. Epilepsia 2004;45:441–451. [PubMed: 15101825]
7. Dombrowski SM, Desai SY, Marroni M, Cucullo L, Goodrich K, Bingaman W, et al. Overexpression of multiple drug resistance genes in endothelial cells from patients with refractory epilepsy. Epilepsia 2001;42:1501–1506. [PubMed: 11879359]
8. Tishler DM, Weinberg KI, Hinton DR, Barbaro N, Annett GM, Raffel C. MDR1 gene expression in brain of patients with medically intractable epilepsy. Epilepsia 1995;36:1–6. [PubMed: 8001500]
9. de Klerk OL, Willemsen AT, Roosink M, Bartels AL, Hendrikse HN, Bosker FJ, et al. Locally increased P-glycoprotein function in major depression: a PET study with [^{11}C]verapamil as a probe for P-glycoprotein function in the blood-brain barrier. Int J Neuropsychopharmacol 2009;19:1–10. [PubMed: 19224656]
10. Kortekaas R, Leenders KL, van Oostrom JC, Vaalburg W, Bart J, Willemsen AT, et al. Blood-brain barrier dysfunction in parkinsonian midbrain in vivo. Ann Neurol 2005;57:176–179. [PubMed: 15668963]
11. Vogelgesang S, Warzok RW, Cascorbi I, Kunert-Keil C, Schroeder E, Kroemer HK, et al. The role of P-glycoprotein in cerebral amyloid angiopathy; implications for the early pathogenesis of Alzheimer's disease. Curr Alzheimer Res 2004;1:121–125. [PubMed: 15975076]
12. Bartels AL, Kortekaas R, Bart J, Willemsen AT, de Klerk OL, de Vries JJ, et al. Blood-brain barrier P-glycoprotein function decreases in specific brain regions with aging: A possible role in progressive neurodegeneration. Neurobiol Aging 2009;30:1818–1824. [PubMed: 18358568]
13. Bauer M, Karch R, Neumann F, Abrahim A, Wagner CC, Kletter K, et al. Age dependency of cerebral P-gp function measured with (*R*)-[^{11}C]verapamil and PET. Eur J Clin Pharmacol 2009;65:941–946. [PubMed: 19655132]
14. Toornvliet R, van Berckel BN, Luurtsema G, Lubberink M, Geldof AA, Bosch TM, et al. Effect of age on functional P-glycoprotein in the blood-brain barrier measured by use of (*R*)-[(^{11})C]verapamil and positron emission tomography. Clin Pharmacol Ther 2006;79:540–548. [PubMed: 16765142]
15. Desrayaud S, Guntz P, Scherrmann JM, Lemaire M. Effect of the P-glycoprotein inhibitor, SDZ PSC 833, on the blood and brain pharmacokinetics of colchicine. Life Sci 1997;61:153–163. [PubMed: 9217274]
16. Schinkel AH, Wagenaar E, van Deemter L, Mol CA, Borst P. Absence of the mdr1a P-Glycoprotein in mice affects tissue distribution and pharmacokinetics of dexamethasone, digoxin, and cyclosporin A. J Clin Invest 1995;96:1698–1705. [PubMed: 7560060]
17. Goldschmidt RB, Steward O. Neurotoxic effects of colchicine: differential susceptibility of CNS neuronal populations. Neuroscience 1982;7:695–714. [PubMed: 7070670]
18. Spiehler VR. Regional distribution of digoxin in the human brain: implications for neurotoxicity. Proc West Pharmacol Soc 1982;25:79–82. [PubMed: 7122544]
19. Sasongko L, Link JM, Muzi M, Mankoff DA, Yang X, Collier AC, et al. Imaging P-glycoprotein transport activity at the human blood-brain barrier with positron emission tomography. Clin Pharmacol Ther 2005;77:503–514. [PubMed: 15961982]
20. Muzi M, Mankoff DA, Link JM, Shoner S, Collier AC, Sasongko L, et al. Imaging of cyclosporine inhibition of P-glycoprotein activity using ^{11}C-verapamil in the brain: studies of healthy humans. J Nucl Med 2009;50:1267–1275. [PubMed: 19617341]
21. Gibaldi, M.; Perrier, B. Pharmacokinetics. 2nd ed.. New York: Marcel Dekker; 1982. p. 319-351.
22. Liow JS, Kreisl W, Zoghbi SS, Lazarova N, Seneca N, Gladding RL, et al. P-glycoprotein function at the blood-brain barrier imaged using ^{11}C-N-desmethyl-loperamide in monkeys. J Nucl Med 2009;50:108–115. [PubMed: 19091890]
23. Homolya L, Hollo Z, Germann UA, Pastan I, Gottesman MM, Sarkadi B. Fluorescent cellular indicators are extruded by the multidrug resistance protein. J Biol Chem 1993;268:21493–21496. [PubMed: 8104940]
24. Raviv Y, Pollard HB, Bruggemann EP, Pastan I, Gottesman MM. Photosensitized labeling of a functional multidrug transporter in living drug-resistant tumor cells. J Biol Chem 1990;265:3975–3980. [PubMed: 1968065]

25. Shapiro AB, Ling V. Stoichiometry of coupling of rhodamine 123 transport to ATP hydrolysis by P-glycoprotein. Eur J Biochem 1998;254:189–193. [PubMed: 9652413]
26. Stein WD. Kinetics of the multidrug transporter (P-glycoprotein) and its reversal. Physiol Rev 1997;77:545–590. [PubMed: 9114823]
27. Aller SG, Yu J, Ward A, Weng Y, Chittaboina S, Zhuo R, et al. Structure of P-glycoprotein reveals a molecular basis for poly-specific drug binding. Science 2009;323:1718–1722. [PubMed: 19325113]
28. Ito H, Kanno I, Fukuda H. Human cerebral circulation: positron emission tomography studies. Ann Nucl Med 2005;19:65–74. [PubMed: 15909484]
29. Raichle ME, MacLeod AM, Snyder AZ, Powers WJ, Gusnard DA, Shulman GL. A default mode of brain function. Proc Natl Acad Sci U S A 2001;98:676–682. [PubMed: 11209064]
30. Seneca N, Zoghbi SS, Liow JS, Kreisl W, Herscovitch P, Jenko K, et al. Human brain imaging and radiation dosimetry of ^{11}C-N-desmethyl-loperamide, a PET radiotracer to measure the function of P-glycoprotein. J Nucl Med 2009;50:807–813. [PubMed: 19372478]
31. Baehr C, Reichel V, Fricker G. Choroid plexus epithelial monolayers--a cell culture model from porcine brain. Cerebrospinal Fluid Res 2006;3:13. [PubMed: 17184532]
32. Rao VV, Dahlheimer JL, Bardgett ME, Snyder AZ, Finch RA, Sartorelli AC, et al. Choroid plexus epithelial expression of MDR1 P-glycoprotein and multidrug resistance-associated protein contribute to the blood–cerebrospinal-fluid drug-permeability barrier. Proc Natl Acad Sci USA 1999;96:3900–3905. [PubMed: 10097135]
33. Hendrikse NH, Schinkel AH, de Vries EG, Fluks E, Van der Graaf WT, Willemsen AT, et al. Complete in vivo reversal of P-glycoprotein pump function in the blood-brain barrier visualized with positron emission tomography. Br J Pharmacol 1998;124:1413–1418. [PubMed: 9723952]
34. Hsiao P, Sasongko L, Link JM, Mankoff DA, Muzi M, Collier AC, et al. Verapamil P-glycoprotein transport across the rat blood-brain barrier: cyclosporine, a concentration inhibition analysis, and comparison with human data. J Pharmacol Exp Ther 2006;317:704–710. [PubMed: 16415090]
35. Chung FS, Eyal S, Muzi M, Link JM, Mankoff DA, Kaddoumi A, et al. PET imaging of tissue P-gp activity during pregnancy in the nonhuman primate. Br J Pharmacol 2010 Jan 1;159(2):394–404. Epub 2009 Dec 4. [PubMed: 20002098]
36. Eyal S, Chung FS, Muzi M, Link JM, Mankoff DA, Kaddoumi A, et al. Simultaneous PET imaging of P-plycoprotein inhibition in multiple tissues in the pregnant non-human primate. J Nucl Med 2009;50:798–806. [PubMed: 19403878]
37. Lee YJ, Maeda J, Kusuhara H, Okauchi T, Inaji M, Nagai Y, et al. In vivo evaluation of P-glycoprotein function at the blood-brain barrier in nonhuman primates using [^{11}C]verapamil. J Pharmacol Exp Ther 2006;316:647–653. [PubMed: 16293715]
38. Bhatti M, Foster R. Pharmacokinetics of the enantiomers of verapamil after intravenous and oral administration of racemic verapamil in a rat model. Biopharm Drug Dispos 1997;18:387–396. [PubMed: 9210977]
39. Nelson W, Olsen L. Regiochemistry and enantioselectivity in the oxidative N-dealkylation of verapamil. Drug Metab Dispos 1988;16:834–841. [PubMed: 2907462]
40. Luurtsema G, Molthoff CF, Windhorst AD, Smit JW, Keizer H, Boellaard R, et al. (R)-and (S)-[^{11}C]verapamil as PET-tracers for measuring P-glycoprotein function: in vitro and in vivo evaluation. Nucl Med Biol 2003;30:747–751. [PubMed: 14499333]
41. Franssen EJ, Luurtsema G, Lammertsma AA. Imaging P-glycoprotein at the human blood-brain barrier. Clin Pharmacol Ther 2006;80:302–303. author reply 3–4. [PubMed: 16952498]
42. Kimchi-Sarfaty C, Oh JM, Kim IW, Sauna ZE, Calcagno AM, Ambudkar SV, et al. A "silent" polymorphism in the MDR1 gene changes substrate specificity. Science 2007;315:525–528. [PubMed: 17185560]
43. Woodahl EL, Crouthamel MH, Bui T, Shen DD, Ho RJ. MDR1 (ABCB1) G1199A (Ser400Asn) polymorphism alters transepithelial permeability and sensitivity to anticancer agents. Cancer Chemother Pharmacol 2009;64:183–188. [PubMed: 19123050]
44. Woodahl EL, Yang Z, Bui T, Shen DD, Ho RJ. MDR1 G1199A polymorphism alters permeability of HIV protease inhibitors across P-glycoprotein-expressing epithelial cells. AIDS 2005;19:1617–1625. [PubMed: 16184031]

45. Brunner M, Langer O, Sunder-Plassmann R, Dobrozemsky G, Muller U, Wadsak W, et al. Influence of functional haplotypes in the drug transporter gene *ABCB1* on central nervous system drug distribution in humans. Clin Pharmacol Ther 2005:182–190. [PubMed: 16084852]

46. Grosset KA, Grosset DG. Prescribed drugs and neurological complications. J Neurol Neurosurg Psychiatry 2004;75 Suppl 3:iii2–iii8. [PubMed: 15316038]

47. Unadkat JD, Chung F, Sasongko L, Whittington D, Eyal S, Mankoff D, et al. Rapid solid-phase extraction method to quantify [^{11}C]-verapamil, and its [^{11}C]-metabolites, in human and macaque plasma. Nucl Med Biol 2008;35:911–917. [PubMed: 19026953]

48. Hebert MF, Easterling TR, Kirby B, Carr DB, Buchanan ML, Rutherford T, et al. Effects of pregnancy on CYP3A and P-glycoprotein activities as measured by disposition of midazolam and digoxin: a University of Washington specialized center of research study. Clin Pharmacol Ther 2008;84:248–253. [PubMed: 18288078]

49. Asano T, Takahashi KA, Fujioka M, Inoue S, Okamoto M, Sugioka N, et al. ABCB1 C3435T and G2677T/A polymorphism decreased the risk for steroid-induced osteonecrosis of the femoral head after kidney transplantation. Pharmacogenetics 2003;13:675–682. [PubMed: 14583680]

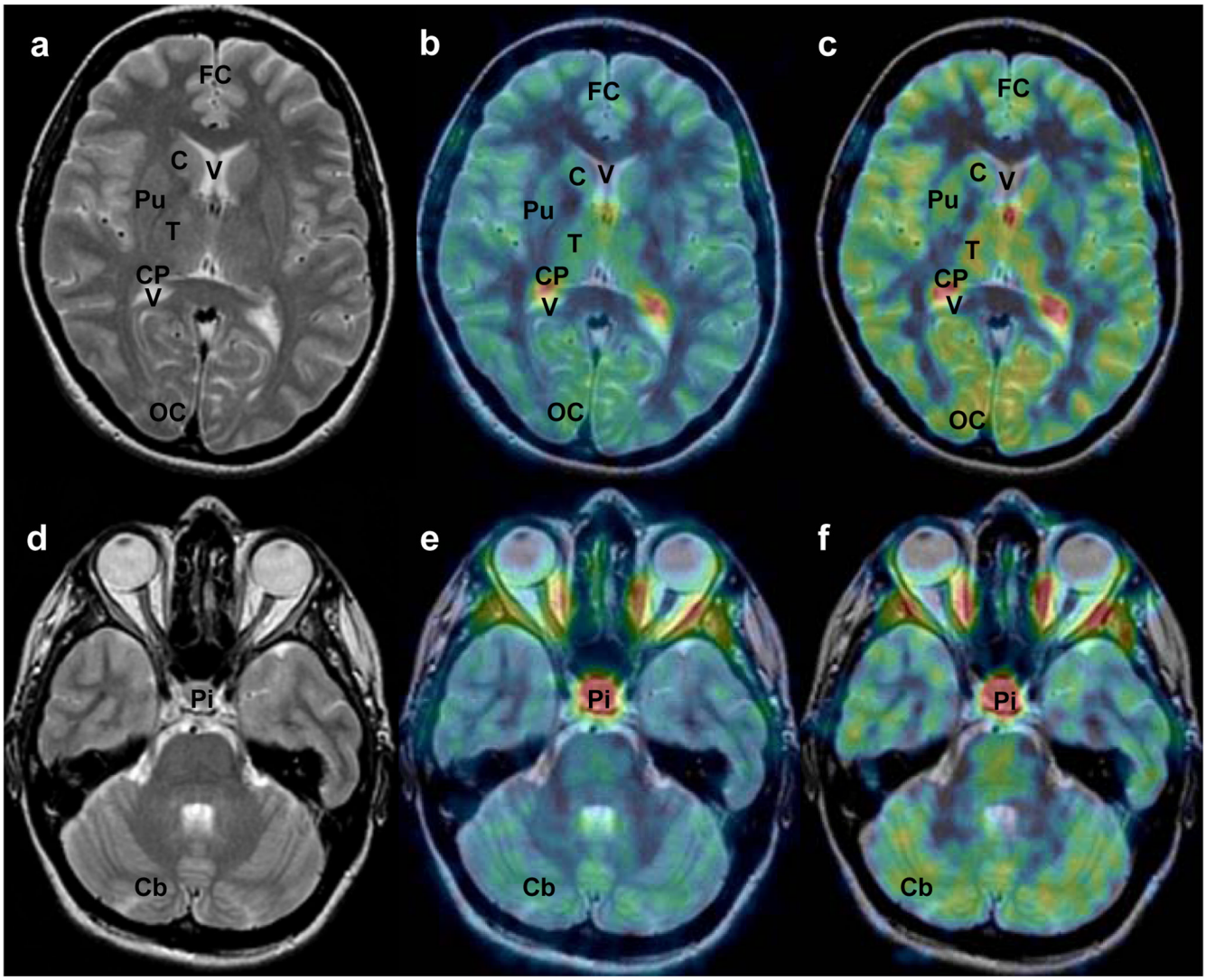

FIGURE 1.

Representative PET co-registered to MR images showing the distribution of radioactivity in human brains after the administration of [^{11}C]-verapamil before (B,E) and during (C,F) cyclosporine infusion (2.5 mg/kg/hr). The MR images are shown in the left panel. C, caudate nucleus; Cb, cerebellum; FC, frontal cortex; OC, occipital cortex; Pu, putamen; Pi, pituitary; T, thalamus, V, lateral ventricle. Images B and C, and E and F were scaled to the same pixel value.

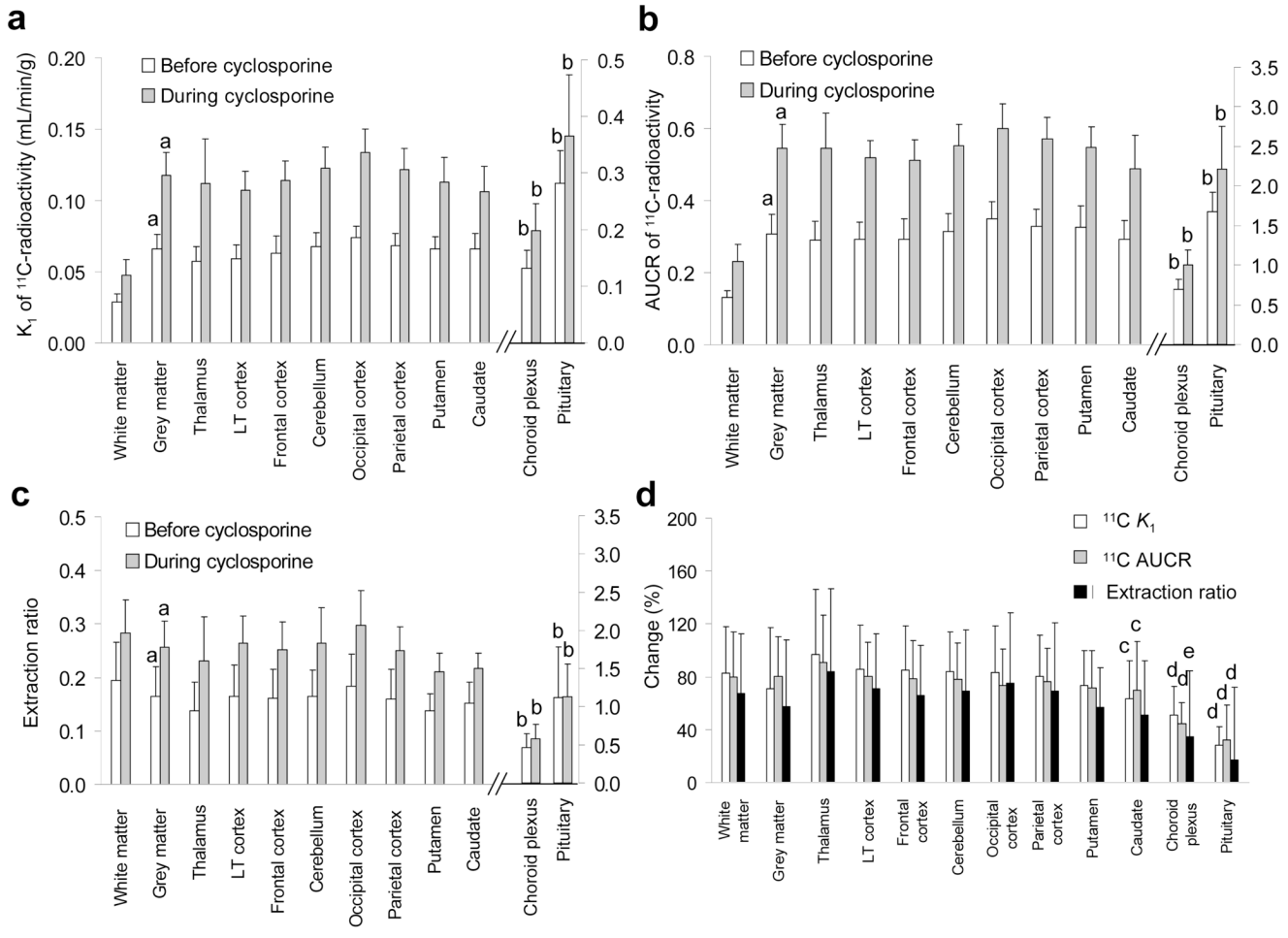

FIGURE 2.

K_1 estimates in both the absence and the presence of cyclosporine, were significantly different between grey and the white matter ([a]; $P < .05$). However, there were no differences in K_1 between the various grey matter regions of the brain. In contrast, the K_1 values of regions of brain not protected by the BBB (choroid plexus and pituitary) were significantly higher than in the lateral temporal cortex or the thalamus ([b]; $P < .05$). In each brain region (including the choroid plexus and the pituitary, right Y-axis), cyclosporine significantly ($P < .01$) increased the K_1 estimate (not marked) (A). Parallel differences were observed in AUCR (B). The differences between the white and grey matter in K_1 were considerably diminished when the ability of the various regions of the brain to extract [^{11}C]-verapamil (ER = K1/rCBF) was examined. In addition, the cyclosporine-induced change in ER was not observed in the choroid plexus and the pituitary (right Y-axis; not marked) (C). The magnitude of cyclosporine-induced changes in K_1 estimates, AUCR and ER was overall similar in all the BBB-protected brain regions. However, the changes in K_1 and AUCR were significantly lower for the caudate nucleus vs. the thalamus ([c], $P < .05$). The changes in the pituitary or the choroid plexus K_1 and AUCR, as well as the pituitary ER, were smaller then in the thalamus or the lateral temporal cortex ([d], $P < .05$). The change in the choroid plexus ER was smaller than in the thalamus ([e], $P < .05$) (D). Data are expressed as mean ± SD (n = 11) and were analyzed by repeated measured ANOVA with Bonferroni's correction or paired *t* test, as appropriate (see Methods). K_1,

distributional clearance; AUCR, the vascular volume-corrected brain/blood ratio of the area of [^{11}C]-radioactivity concentration-time curve from 0 to 10 min; LT, lateral temporal.

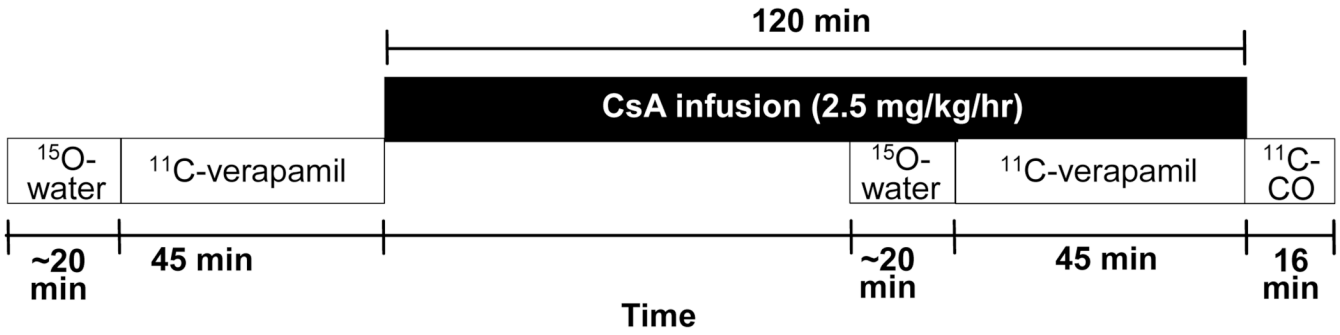

FIGURE 3.

A schematic of the PET imaging protocol used to study the healthy volunteers. The imaging protocol consisted of 5 sub-studies: ^{15}O-water (before cyclosporine infusion, for evaluation of regional cerebral blood flow), ^{11}C-verapamil (before cyclosporine infusion, for evaluation of regional P-gp activity at the BBB), ^{15}O-water (during cyclosporine infusion, approximately 1 hr after onset of the cyclosporine infusion), ^{11}C-verapamil (during cyclosporine infusion), and ^{11}C-CO (for evaluation of tissue vascular volume).

TABLE 1

ABCB1 genotype and grey and white matter ER (K_1/rCBF) of [^{11}C]-radioactivity before and during the administration of cyclosporine (2.5 mg/kg/hr).

Subject	Sex	Genotype				Grey matter ER of [^{11}C]-radioactivity			White matter ER of [^{11}C]-radioactivity		
		3435	2677	1236	1199	Without cyclosporine	With cyclosporine	Change (%)	Without cyclosporine	With cyclosporine	Change (%)
2104	F	C/C	G/G	C/T	G/G	0.193	0.289	49	0.176	0.325	84
2107	F	C/T	G/T	C/T	G/G	0.122	0.228	87	0.154	0.176	14
2108	F	C/T	G/T	C/T	G/G	0.156	0.270	73	0.187	0.276	48
2099	F	C/T	G/T	C/T	G/G	0.084	0.217	159	0.135	0.219	63
2070	M	C/C	G/G	C/T	G/G	0.145	0.235	63	0.163	0.320	96
2083	M	C/C	G/G	T/T	G/G	0.207	0.382	84	0.326	0.402	23
2081	M	T/T	T/T	C/C	G/G	0.132	0.231	76	0.161	0.293	82
2090	M	T/T	T/T	C/C	G/G	0.259	0.258	0	0.321	0.290	−10
2110	M	C/T	G/T	C/T	G/G	0.191	0.275	45	0.211	0.316	49